

Likely detection of water-rich asteroid debris in a metal-polluted white dwarf

R. Raddi^{1*}, B.T. Gänsicke¹, D. Koester², J. Farihi³, J.J. Hermes¹,
S. Scaringi⁴, E. Breedt¹, J. Girven¹

¹ *Department of Physics, University of Warwick, Gibbet Hill Road, Coventry CV4 7AL, UK*

² *Institut für Theoretische Physik und Astrophysik, University of Kiel, 24098 Kiel, Germany*

³ *University College London, Dept. of Physics & Astronomy, London, WC1E 6BT, UK*

⁴ *Max Planck Institut für Astrophysik, Karl-Schwarzschild-Str. 1, 85748, Garching, Germany*

Accepted 2015 March 26. Received 2015 March 18; in original form 2015 February 18

ABSTRACT

The cool white dwarf SDSS J124231.07+522626.6 exhibits photospheric absorption lines of 8 distinct heavy elements in medium resolution optical spectra, notably including oxygen. The $T_{\text{eff}} = 13\,000\text{ K}$ atmosphere is helium-dominated, but the convection zone contains significant amounts of hydrogen and oxygen. The four most common rock-forming elements (O, Mg, Si, and Fe) account for almost all the accreted mass, totalling at least $1.2 \times 10^{24}\text{ g}$, similar to the mass of Ceres. The time-averaged accretion rate is $2 \times 10^{10}\text{ g s}^{-1}$, one of the highest rates inferred among all known metal-polluted white dwarfs. We note a large oxygen excess, with respect to the most common metal oxides, suggesting that the white dwarf accreted planetary debris with a water content of ≈ 38 per cent by mass. This star, together with GD 61, GD 16, and GD 362, form a small group of outliers from the known population of evolved planetary systems accreting predominantly dry, rocky debris. This result strengthens the hypothesis that, integrated over the cooling ages of white dwarfs, accretion of water-rich debris from disrupted planetesimals may significantly contribute to the build-up of trace hydrogen observed in a large fraction of helium-dominated white dwarf atmospheres.

Key words: stars: white dwarfs - individual: SDSS J124231.07+522626.6 - stars: abundances - planetary systems

1 INTRODUCTION

There is now evidence that at least 20–30 per cent of all white dwarfs with cooling ages $\gtrsim 100\text{ Myr}$ have preserved parts of their planetary systems throughout the post-main sequence evolution (Zuckerman et al. 2003, 2010; Koester et al. 2014), via detection of trace metals in their otherwise pure hydrogen and helium atmospheres (e.g. Koester et al. 2005; Dufour et al. 2007). These evolved planetary systems provide detailed information on the frequency, architecture, and chemical composition of extra solar planetary systems, once orbiting early F-, A-, and late B-type stars of $\approx 1.2\text{--}3 M_{\odot}$.

Since the strong surface gravity of white dwarfs results in the radial stratification of their chemical constituents (Schatzman 1945, 1947), the heavy elements detected in the spectra of some white dwarfs must come from an external source (Dupuis et al. 1992, 1993). The thermal emission from circumstellar dust has been detected in the infrared at

about 35 white dwarfs (Reach et al. 2005; Kilic et al. 2006; Jura et al. 2007; Farihi et al. 2009; Bergfors et al. 2014), some of which show line emission from a gaseous component (e.g. Gänsicke et al. 2006, 2008; Farihi et al. 2012a; Melis et al. 2012; Wilson et al. 2014). Circumstellar debris discs at white dwarfs are thought to form after the tidal disruption of planetesimals (Debes & Sigurdsson 2002; Jura 2003; Veras et al. 2014a).

To date only a handful of white dwarfs have been observed for detailed composition analysis, but for these stars the bulk composition of the planetesimals causing metal-pollution has been inferred to be similar to that of the inner Solar System, with the four most common rock-forming elements (O, Mg, Si, Fe) being the dominant species (Zuckerman et al. 2007; Klein et al. 2010; Vennes et al. 2010; Gänsicke et al. 2012, see also Jura & Young 2014 for a review). Furthermore, the diverse composition exhibited by polluted white dwarfs, specifically with respect to the relative abundances of iron, siderophile, and refractory elements, also indicates melting, stripping and core differentiation of extra solar asteroids (e.g. Melis et al. 2011). In most of the

* E-mail: r.raddi@warwick.ac.uk

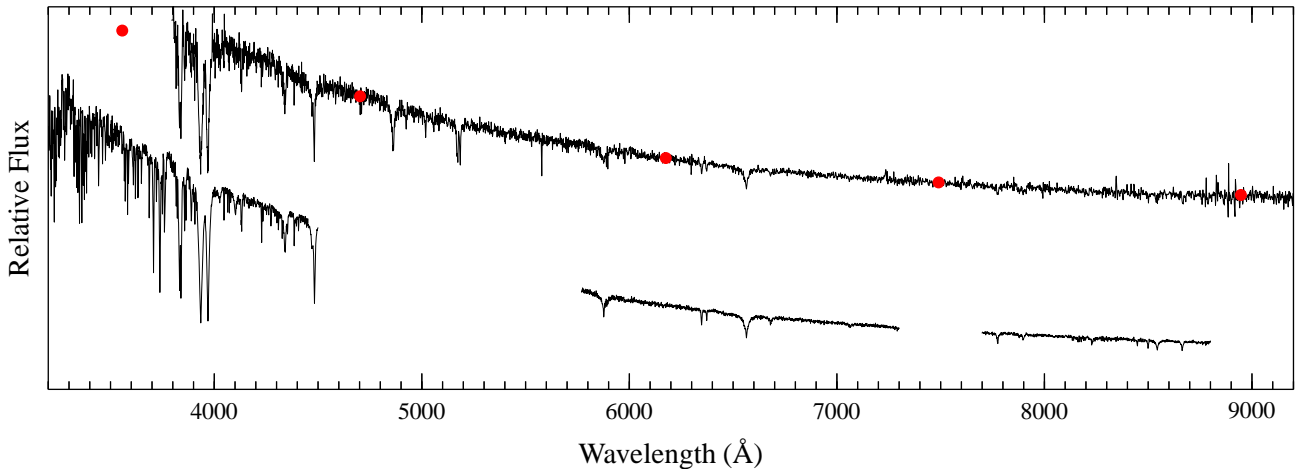


Figure 1. Comparison between the SDSS (top) and WHT/ISIS (bottom) spectra of SDSS J1242, offset with respect to each other. The wavelength coverage of the WHT/ISIS observations is more fragmentary, due to the adopted dual-arm configuration that causes the gaps at 4500–5700 Å, and 7300–7700 Å. However, the data extend to shorter ultraviolet wavelengths and offer improved signal-to-noise ratio up to a factor of 5 times better than the SDSS spectrum. The SDSS broad-band photometry (in Table 1) is also overplotted, as filled red dots, on to the SDSS spectrum.

cases, the polluting debris appears to be notably depleted of volatile elements such as H, C, N, and S, and generally drier than Solar System CI chondrites (e.g. Jura 2006; Klein et al. 2011).

The presence of water in exoplanets is crucial in the context of life outside the Solar System. White dwarfs offer a unique insight into the ubiquity of water. Farihi et al. (2013) presented the first unambiguous evidence for ongoing accretion of water-rich debris in GD 61. The helium-dominated atmosphere of this white dwarf contains a large mass of hydrogen, although not unusual for stars of similar temperature, but the inferred mass of oxygen exceeds what is expected from the accretion of metal oxides. This suggests that the parent body contained 26 per cent of water by mass. Two other helium-dominated white dwarfs, GD 16 and GD 362, were also discussed in the context of accretion from water-rich debris (e.g. Jura 2008; Jura et al. 2009; Jura & Xu 2010), both stars showing circumstellar dust emission that reveals ongoing accretion. However, while the atmospheres of these stars contain larger amounts of hydrogen ($\geq 10^{24}$ g), along with traces of rock-forming metals, the exact origin of hydrogen cannot be unambiguously linked to the circumstellar material.

Here, we present the discovery and follow-up observations of SDSS J124231.07+522626.6 (hereafter SDSS J1242), a metal-polluted helium-dominated white dwarf with strong absorption lines of hydrogen, oxygen and seven other heavy elements. We outline in Section 3.1 the model atmosphere analysis and the determination of element abundances. In Section 3.2, we analyse the infrared data, and comment on the non-detection of circumstellar dust emission. In Section 4, we discuss the composition of the debris polluting the atmosphere of SDSS J1242 and highlight the large oxygen and hydrogen content, suggesting that SDSS J1242 accreted water-rich debris. Finally, we summarise our findings in Section 5.

2 OBSERVATIONS

2.1 Identification based on SDSS data

Optical spectroscopy of SDSS J1242 was obtained by the Sloan Digital Sky Survey (SDSS; York et al. 2000) on 2002 April 15, and released as part of Data Release 2 (DR 2; Abazajian et al. 2004). It was initially classified by Eisenstein et al. (2006) as a subdwarf because of its narrow Balmer and He II lines (Fig. 1). As part of our previous analysis of the Data Release 7 (DR 7; Abazajian et al. 2009), we retained this classification (Girven et al. 2011). Upon closer inspection, we subsequently found the spectrum of SDSS J1242 to resemble those of other metal-polluted white dwarfs, which appear as DAZ¹ spectral types under low resolution spectroscopy, and only high resolution spectroscopy showed helium to be the dominant element in their atmospheres (e.g. GD 362, and GD 16; Zuckerman et al. 2007; Koester et al. 2005). We therefore reclassify here SDSS J1242 as a white dwarf, and obtained follow-up observations.

In Table 1, we report the optical SDSS photometry and the ultraviolet photometry from the Galaxy Evolution Explorer (*GALEX*; Morrissey et al. 2007).

2.2 WHT/ISIS observations

We observed SDSS J1242 with the Intermediate dispersion Spectrograph and Imaging System (ISIS) at the 4.2-m William Herschel Telescope (WHT) in La Palma.

The WHT/ISIS spectra were taken on two occasions, in 2012 May 31, and 2012 December 14. We used a 1 arcsec slit, the standard 5300 dichroic, and the R600B and R600R

¹ We type SDSS J1242 as a DAZB white dwarf, following the spectral classification scheme of Sion et al. (1983). D stands for degenerate star, while A, Z, and B indicate the presence of hydrogen, metallic, and helium lines ordered by line strength.

gratings in the blue and red arm, respectively. The order-sorting filter GG495 was mounted on the red arm. The blue arm covered 3100–4500 Å at a resolution of 1.8 Å. We opted for two different configurations of the red arm, to cover the regions around H α (5800–7300 Å) and Ca II triplet (7700–8800 Å) at a resolution of 2 Å. With this setup, we obtained spectra bluer than the Balmer jump, which were not available from SDSS.

We observed in the blue arm for a total of 4.7 hr, split roughly equally between the two runs. The H α region was exposed for 2.6 hr, while the Ca II region was exposed for 2.3 hr. Spectrophotometric standards and CuAr+CuNe arcs were acquired across the night, for the flux and wavelength calibrations. We had clear sky and 1 arcsec seeing during both runs.

We followed standard data-reduction procedures for removal of the bias, flat field correction, wavelength calibration, extraction of the spectrum, flux calibration and removal of telluric lines. All the reduction steps were undertaken with the PAMELA (Marsh 1989) and MOLLY packages².

The coadded WHT/ISIS spectra and the SDSS spectrum are shown in Fig. 1. The quality of the WHT/ISIS spectra is superior with respect to the SDSS data in terms of wavelength coverage, resolution and signal-to-noise ratio (up to a factor of 5), which we measure to range between 20–40 in the red arm and 80–100 in the blue arm. However, we find the WHT/ISIS spectrum to display 15 per cent more flux in the u -band with respect to the SDSS photometry, probably arising from an imperfect flux calibration.

2.3 Ground based near-infrared photometry

Near-infrared JHK_s photometry was obtained with the Long-slit Intermediate Resolution Infrared Spectrograph (LIRIS, Manchado et al. 1998) at the WHT on 2011 March 23. SDSS J1242 was observed in a continuous and dithered manner in each of the three filters with individual exposure times of 30 s in J , and H , and 20 s in K_s , for a total integration time of 540 s in each filter. Three standard star fields from the ARNICA catalogue (Hunt et al. 1998) were observed for flux calibration. The median sky subtracted frames were shifted and average combined into a single image per filter on which aperture photometry was performed with IRAF tasks. The aperture radii used for the flux standard were $r = 3''.75$ with $5''.0$ – $7''.5$ sky annuli, while smaller apertures of $1''.25$ were used for the science target, and corrected using several bright stars in each reduced frame. The absolute flux calibration was good to 5 per cent or better, and the resulting JHK_s photometry is listed in Table 1.

2.4 Spitzer IRAC observations

SDSS J1242 was observed on 2013 June 26 with the *Spitzer* warm mission (Werner et al. 2004) as part of Cycle 9 program 90121. Images of the science target were taken using the Infrared Array Camera (IRAC; Fazio et al. 2004) at

Table 1. Multi-wavelength photometry for SDSS J1242.

Source	λ_{eff} [μm]	m [(AB) mag]	F_ν [μJy]
<i>GALEX</i>	0.15	21.0 ± 0.3	14 ± 3
<i>GALEX</i>	0.23	18.91 ± 0.06	99 ± 10
SDSS u	0.36	17.87 ± 0.03	270 ± 14
SDSS g	0.47	17.74 ± 0.02	291 ± 15
SDSS r	0.62	17.96 ± 0.02	238 ± 12
SDSS i	0.75	18.19 ± 0.02	191 ± 10
SDSS z	0.89	18.38 ± 0.04	157 ± 8
LIRIS J	1.24	18.15 ± 0.05	87 ± 4
LIRIS H	1.66	18.12 ± 0.05	58 ± 3
LIRIS K_s	2.16	18.06 ± 0.05	40 ± 2
IRAC	3.55	18.15 ± 0.06	15.5 ± 0.7
IRAC	4.49	18.25 ± 0.06	9.0 ± 0.5

both 3.6 and 4.5 μm , in a series of 30 s exposures with 40 medium size dithers in the cycling pattern, for a total exposure time in each channel of 1200 s. Fully reduced, combined, and flux-calibrated images were analysed following Farihi et al. (2010b) using 0.6 pixel⁻¹ mosaics created using MOPEX. Aperture photometry was performed with tasks in IRAF using $r = 4$ pixel radii and 24–40 pixel sky annuli, applying aperture corrections recommended in the IRAC Instrument Handbook. The IRAC photometry is listed in Table 1 and shown in Figure 3, where errors include the standard deviation in the sky annuli and an additional 5 per cent absolute calibration uncertainty.

3 SPECTRAL AND ENERGY DISTRIBUTION ANALYSIS

3.1 Spectral modelling

A first determination of the stellar parameters was obtained from the SDSS spectrum and photometry. The input physics of the stellar models that we used has been described extensively in Koester (2010). Since both hydrogen and helium lines are detected in the spectrum, we prepared a grid of models with different H/He abundances. These models include both Stark broadening by electrons and He⁺ ions, and neutral broadening by He atoms. Due to the intrinsic difficulty in measuring the effect of surface gravity on spectral lines for helium-rich atmospheres in this range of T_{eff} , we initially fixed $\log g = 8$, which corresponds to a typical 0.59 M_\odot white dwarf (e.g. Tremblay et al. 2013, and references therein). The best-fit temperature was 12 500 K. We also obtained initial abundance determinations for the elements that are visible in the SDSS spectrum: O, Na, Mg, Si, Ca, and Fe.

The best-fitting model was subsequently compared to the WHT/ISIS spectra that are suitable for a more detailed chemical analysis. We first noted that $T_{\text{eff}} = 13 000 \pm 300$ K better reproduces the ionisation equilibria for the observed elements. Next, we adjusted the initial abundances in steps of 0.1 dex in order to improve individual abundances and error estimates for elements that have well-isolated lines (verified by visual assessment as in Gänsicke et al. 2012). This was possible for H, O, Na, Mg, Si, and Ca. The abundances of Ti, Cr, and Fe, which have many overlapping lines in the

² Both developed by T. R. Marsh. PAMELA is part of the STARLINK distribution at <http://starlink.jach.hawaii.edu/starlink>. MOLLY is available at <http://www.warwick.ac.uk/go/trmarsh/software/>.

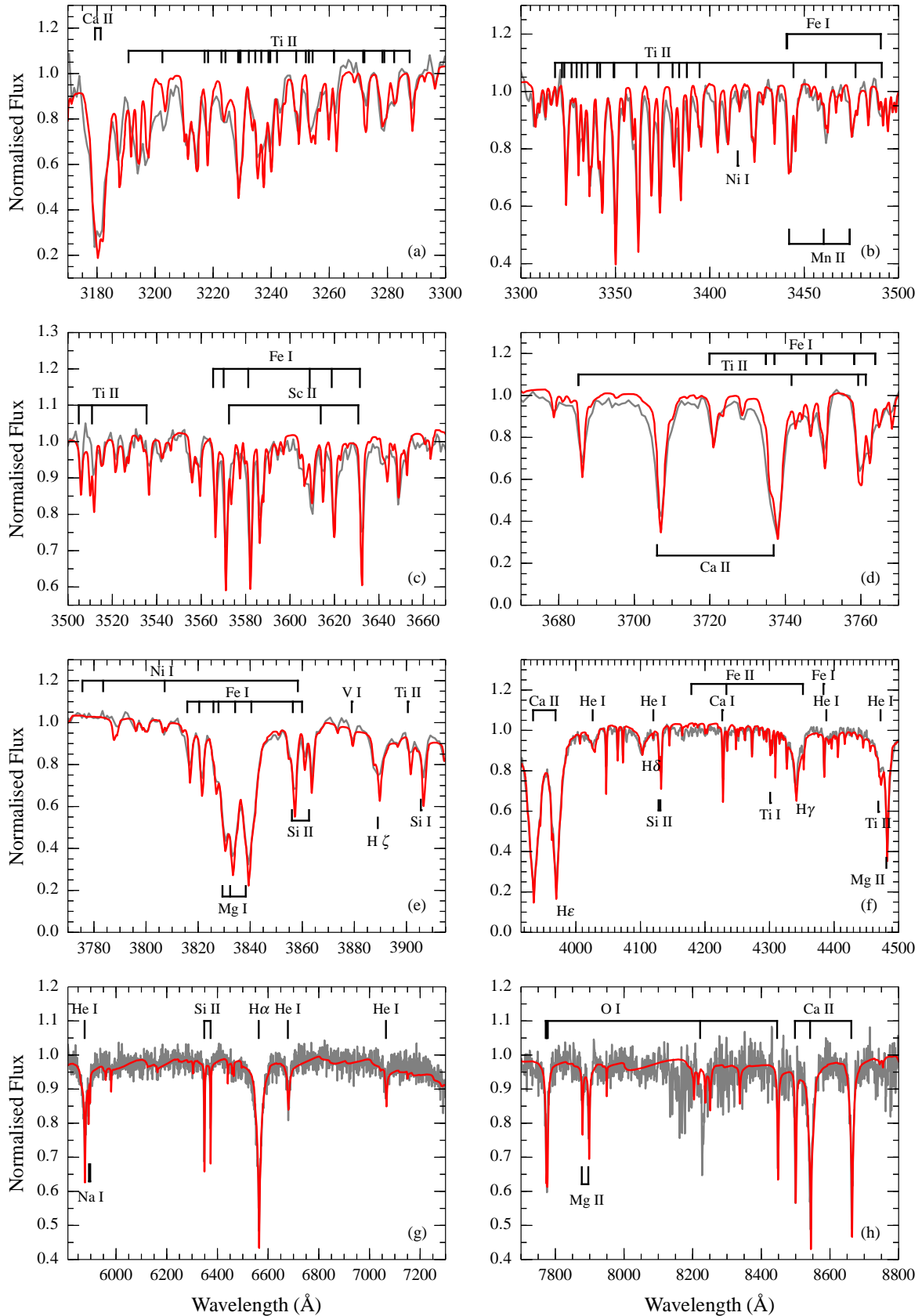


Figure 2. WHT/ISIS spectrum (grey) and best-fit model atmosphere (red) with $T_{\text{eff}} = 13\,000\text{ K}$ and $\log g = 8$. In panel (h), a problematic sky subtraction causes the noisier appearance of the spectrum at $8100\text{--}8300\text{ \AA}$.

Table 2. Photospheric element abundances derived from the WHT/ISIS spectrum, adopting $T_{\text{eff}} = 13\,000\text{ K}$, and $\log g = 8$.

Z	Element	$[Z/\text{He}]$
1	H	-3.68 ± 0.10
6	C	< -4.70
7	N	< -5.00
8	O	-4.30 ± 0.10
11	Na	-7.20 ± 0.20
12	Mg	-5.26 ± 0.15
13	Al	< -6.50
14	Si	-5.30 ± 0.06
15	P	< -6.60
16	S	< -8.00
20	Ca	-6.53 ± 0.10
21	Sc	< -9.50
22	Ti	-8.20 ± 0.20
23	V	< -9.00
24	Cr	-7.50 ± 0.20
25	Mn	< -8.00
26	Fe	-5.90 ± 0.15
28	Ni	< -7.30

3200–3700 Å range, were determined globally using regions where always one of the three elements is dominant.

The WHT/ISIS spectrum along with the best-fit model are displayed in Fig. 2. We note a complex of Ti II lines in the range 3300–3800 Å, from which we determine precise abundances for this element. Fe I, Fe II, Mn I, and strong ultraviolet Ca II lines, in addition to Ca II H & K, are also evident in the blue spectrum. Other strong absorption lines that were already detected in the SDSS spectrum appear much more structured at the higher resolution and better signal-to-noise ratio of the WHT/ISIS data, in particular Na I D, Si II, O I, Mg II, and Ca II triplet in the red spectra. For a comprehensive list of the most important transitions, which are labelled Fig. 2, see also Klein et al. (2011).

Only upper limits could be determined for C, N, Al, P, S, Sc, V, Mn, and Ni. Since these limits were in all cases larger than their solar abundances, we included them in the model calculations fixed to solar ratios and verified that the inclusion did not have significant influence on the fit. The final abundances were then determined statistically, using the standard width of the distribution from fits to different lines as error estimate, and are summarised in Table 2.

From the WHT/ISIS spectrum we also have estimated how a different surface gravity influences the measurement of the metal abundances. In fact, the ionisation balance is affected by the surface gravity and is coupled to the electron density, while the line strengths depends also on the neutral density via the line broadening. Helium-dominated white dwarfs are suspected to have masses in the range 0.67–0.74 M_{\odot} (Bergeron et al. 2011; Falcon et al. 2012), which correspond to slightly larger surface gravities than the canonical $\log g = 8$ that we adopted. However, we cannot exclude SDSS J1242 to be less massive than 0.60 M_{\odot} , therefore we altered $\log g$ by ± 0.25 dex, which spans the mass range of most known white dwarfs (see Tremblay et al. 2013), i.e. 0.45–0.80 M_{\odot} . The unknown surface gravity induces systematic uncertainties of 0.02–0.07 dex for H, Na, Mg, and Fe, and up to 0.2 dex for O. The effect that different surface gravities have on the relative abundance ratios is discussed

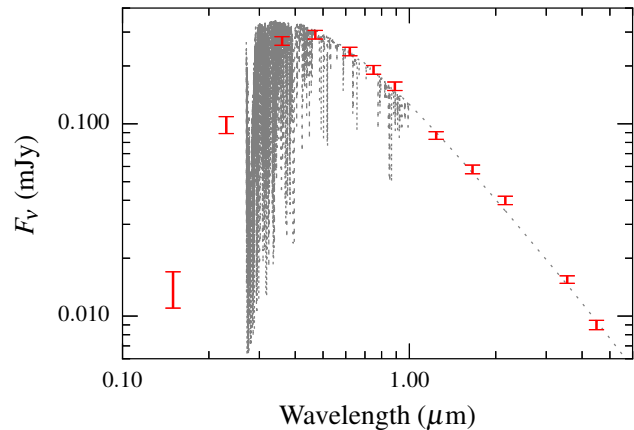


Figure 3. The model atmosphere with $T_{\text{eff}} = 13\,000\text{ K}$, $\log g = 8$ is shown. The error bars represent the broad-band photometry given in Table 1.

in Section 4.1, where we consider the diffusion of elements in the convection zone of SDSS J1242.

We have estimated the interstellar reddening $E(B-V)$, measuring the colour excess in the optical. This is computed with respect to the synthetic colours determined from the best-fit model, which are: $(u-g) = -0.041$, $(g-r) = -0.238$, $(r-i) = -0.238$, and $(i-z) = -0.286$. We obtain $E(B-V) = 0.05 \pm 0.02$, which agrees within 2σ with the total Galactic reddening measured along the line-of-sight to SDSS J1242 ($E(B-V) \approx 0.015$, Schlegel et al. 1998). We determine a spectroscopic parallax of 164 ± 28 pc, using the absolute g magnitude scale for DB white dwarfs by Bergeron et al. (2011) and $A(g) = 3.77 \times E(B-V) = 0.19$ from the standard Cardelli et al. (1989) reddening law.

3.2 Search for dust emission in the infrared

In Fig. 3 we display all available photometry for SDSS J1242, including the ground- and space-based data from the ultraviolet through the infrared. The data are overplotted with the best fitting atmospheric model as described in the previous section.

It is noteworthy that the K_s -band data point lies about 2σ above the predicted photosphere, and the JHK_s colours appear redder than the model slope. The flux calibration for the JHK_s photometry was scrutinised for possible sources of error, and while none were found, there was only a single, faint 2MASS point source in the LIRIS field for an independent zero point determination. Given the IRAC fluxes, which are both self consistent and relatively robust in accuracy, the conclusion must be the JHK_s fluxes contain some, modest additional error.

As can be seen from the figure, relative to the model there is no excess infrared emission that might originate in circumstellar dust. While an in-depth discussion of the detectability of discs at white dwarfs is beyond the scope of this paper, because the accretion history of SDSS J1242 influences the forthcoming interpretation of the observed heavy elements, a brief discussion is useful here. First and most relevant is that narrow rings of solid material holding up to 10^{22} g can remain undetected at white dwarfs for incli-

Table 3. Physical parameters of SDSS J1242.

Parameters	$T_{\text{eff}} = 13\,000 \pm 300\text{ K}$		
	$\log g = 7.75$	$\log g = 8.00$	$\log g = 8.25$
Mass (M_{\odot})	0.48	0.59	0.75
Radius (R_{\odot})	0.015	0.013	0.011
Cooling age (Gyr)	0.25	0.32	0.50
Distance (pc)	193	164	137
q_{cvz}	-4.9	-5.4	-5.9
$\log M_{\text{H}}$ [g]	23.80	23.38	22.99

nations above 50 degrees (Farihi et al. 2010b). Such rings can account for the highest instantaneous accretion rates, and for the bulk of parent body masses inferred for polluted white dwarfs. Second, a population of narrow rings is indicated by recent *Spitzer* studies that reveal a growing number of subtle infrared excesses (Bergfors et al. 2014), and where the frequency of infrared excesses rises sharply at fainter disc luminosities (Rocchetto et al. 2014).

The implications of the non detection of infrared emission from circumstellar dust become relevant in the following section, where we discuss the likely accretion history for SDSS J1242 and detail the atmospheric composition.

4 DISCUSSION

4.1 Diffusion analysis

White dwarfs with helium-rich (DB) atmospheres develop a convection zone for $T_{\text{eff}} \lesssim 25\,000\text{ K}$ (see fig. 3 in Bergeron et al. 2011). The depth of the convection zone, typically expressed as a fraction of the white dwarf mass, $q_{\text{cvz}} = \log(M_{\text{cvz}}/M)$, depends on the atmospheric parameters T_{eff} and $\log g$. For SDSS J1242, we infer $q_{\text{cvz}} = -5.4$ using the most up-to-date version of the stellar structure computations described in Koester (2009), which adopt the mixing-length approximation (Böhm-Vitense 1958) with a parameter $ML2/\alpha = 1.25$. White dwarf mass, radius, and age are estimated using the DB cooling models of the Montreal group³, for $\log g = 8.00 \pm 0.25$, and are given in Table 3 along with the values of q_{cvz} .

In the atmosphere of a convective white dwarf, elements heavier than hydrogen and helium will eventually diffuse out with time-scales that depend on the atomic weight of the element and the local conditions at the bottom of the convection zone. Given the considerable length of these diffusion time-scales, $\approx 1\text{ Myr}$ in the case of SDSS J1242, variations in the accretion rate on shorter time-scales can result in differences between the photospheric abundances, and those of the accreted debris. Koester (2009) illustrates the accretion on to a white dwarf in a simple fashion, consisting of three phases: i) build-up or early-phase, during which the abundances in the photosphere increase and the relative abundance ratios equal those of the debris; ii) steady-state, when photospheric and debris abundances scale with the relative diffusion velocities, as the equilibrium between accretion and diffusion is reached; iii) declining stage, when the accretion

³ Available at: <http://www.astro.umontreal.ca/~bergeron/CoolingModels/>

Table 4. Diffusion data for SDSS J1242 for the $T_{\text{eff}} = 13\,000\text{ K}$ and $\log g = 8$ model. From left to right: the mass of elements that is mixed in the convection zone, diffusion velocities, diffusion time scales, and mass fluxes (see Koester 2009, for more details).

Element	M_{Z} (10^{23} g)	v 10^{-8} (cm/s)	τ (Myr)	M_{Z} 10^7 (g/s)
C	< 2.8	3.5	2.3	< 371.27
N	< 1.7	3.7	2.2	< 228.91
O	9.6	3.6	2.2	1282.10
Na	0.02	3.7	2.2	2.36
Mg	1.6	3.3	2.4	197.35
Al	< 0.1	3.6	2.2	< 13.49
Si	1.7	4.6	1.7	285.23
P	< 0.09	6.9	1.2	< 23.72
S	< 0.004	7.9	1.0	< 1.13
Ca	0.1	8.0	1.0	42.26
Sc	< 0.0002	8.6	0.9	< 0.05
Ti	0.004	8.5	0.9	1.13
V	< 0.0006	8.4	0.9	< 0.19
Cr	0.02	7.9	1.0	5.72
Mn	< 0.006	7.8	1.0	< 1.90
Fe	0.8	7.4	1.1	228.85
Ni	< 0.03	6.6	1.2	< 8.80
Sum*	12.4			2045.00

*: Upper limits are not included

has stopped and the photospheric abundances decrease exponentially with different diffusion time-scales for each element.

Here, we consider the accretion-diffusion equilibrium, which is the only well-modelled phase, providing a lower limit on the mass of debris that has been accumulated in the convection zone. From diffusion calculations that follow the prescriptions of Koester (2009), we estimate for each detected element the diffusion time-scale, diffusion velocity, and the mass flux throughout the atmosphere – which is equal to the time-averaged accretion rate on to the star. Since the diffusion data depend on the white dwarf mass, we investigate the effect that the uncertainty of $\Delta \log g = \pm 0.25$ dex has on the calculations. We note that a decrease (increase) of 0.25 dex results in: a) 40 per cent decrement (increment) in the average diffusion velocities; b) the mean diffusion time-scales become about 3 times longer (shorter); c) the mean mass fluxes that are required to produce the observed traces of elements in the stellar atmosphere are 20 per cent smaller (larger). We conclude that the diffusion parameters scale uniformly with a change of surface gravity, differing very little for individual elements, of the order of few per cent, from the average scaling. Finally, the mass flux ratios also remain unchanged within a few per cent. Changes induced by the temperature uncertainty are irrelevant in comparison. Therefore, in Table 4 we give the diffusion data relative to $T_{\text{eff}} = 13\,000\text{ K}$ and $\log g = 8$ only.

4.2 Accretion rate and parent body mass

The diffusion analysis makes SDSS J1242 a remarkable object. First, the mass of heavy elements within its convection zone is $1.2 \times 10^{24}\text{ g}$, larger than the mass of Ceres, the largest asteroid in the Solar System which is best described as a fully differentiated, planetary embryo. This is actually a lower limit to the total accreted mass, and makes this star one of the most polluted white dwarfs known. Sec-

ond, the total accretion rate we derive (averaged over the diffusion time-scales of ≈ 1 Myr), of $2 \times 10^{10} \text{ g s}^{-1}$, is also among the highest of all known metal-polluted white dwarfs (Girven et al. 2012; Dufour et al. 2012).

In the case helium-dominated atmospheres with Myr-long diffusion time-scale, ongoing accretion is uncertain in the absence of an infrared excess associated with closely orbiting dust. Furthermore, while the time-averaged accretion rate of SDSS J1242 is set, its accretion history is unknown, and specifically whether the rate has changed over the last one to few metal sinking time-scales. There is some observational evidence that accretion rates change over time, where relatively short bursts of high rates may influence the time-averaged rates for stars like SDSS J1242 (Farihi et al. 2012b).

In the absence of dust detection, it is difficult to construct a scenario in which the accretion on to SDSS J1242 is in the early phase (i.e. where a single diffusion time-scale has not yet passed since the onset). This is because the implications would be either 1) the inferred accretion rate is also the instantaneous rate, and a disc with mass $\gtrsim 10^{24} \text{ g}$ would require an unlikely, near edge-on configuration to escape detection, or 2) an entire planetary body exceeding the mass of Ceres was accreted in a short time (< 1 Myr) and the system is observed at a special epoch. Given the potential for discs to linger for several Myr (Klein et al. 2010; Bochkarev & Rafikov 2011; Girven et al. 2012), it is more likely SDSS J1242 is accreting now at a relatively modest rate compared to its time-averaged rate, and could have formed a disc that is too subtle to be detected in our *Spitzer* data, due to being gas-dominated, narrow, inclined, or a combination of these factors.

Given the 1–2 Myr time-scales for heavy elements to diffuse from the convection zone, the star could be in a declining phase (as opposed to a steady state), where accretion halted at least one diffusion time-scale ago. In that situation, the metal mass present in the outer layers of the star would be decreasing exponentially. If indeed several Myr have passed since the end of the accretion episode, the accreted parent body would have to be more massive than Pluto to account for the currently observed metal abundances. Because the accretion of entire planets is expected to happen only rarely (Veras et al. 2013), such events are unlikely to be detected and a significant passage into a declining phase of accretion can be discounted.

4.3 Composition of the debris

Analysing in detail the atmospheric composition of SDSS J1242, we note that oxygen, magnesium, silicon, and iron (which alone make up 94 per cent of bulk Earth, McDonough 2001), account for 99 per cent by mass of metals we detect. In particular, oxygen is the most abundant element in the photosphere of SDSS J1242, with a mass fraction of 64 ± 13 per cent. Oxygen is followed by magnesium, silicon, and iron with 10 ± 1 , 14 ± 1 , and 11 ± 2 per cent respectively. SDSS J1242 has an iron and magnesium content that is compatible with basaltic rocks typical of a wide array of achondritic meteorites, such as howardites, eucrites, and diogenites (see fig. 6 in Nittler et al. 2004). These compositions result from partial melt or fractional crystallisation of silicate rocks, inducing magnesium enhancement, and are

Table 5. Oxygen mass fraction balance in SDSS J1242

Oxide	Mass Fraction
Na ₂ O	0.0006 ± 0.0002
MgO	0.10 ± 0.02
Al ₂ O ₃	< 0.009
SiO ₂	0.25 ± 0.05
CaO	0.013 ± 0.004
TiO ₂	0.0006 ± 0.0002
Cr ₂ O ₃	0.0021 ± 0.0005
FeO	0.05 ± 0.01
O excess	0.57 ± 0.07
H ₂ O	0.38 ± 0.10

observed on the surface of differentiated asteroids in the Solar System (e.g. Vesta; De Sanctis et al. 2012).

To compare our results to those concerning the bulk composition of Solar System meteorites, we compute the relative weight ratios of magnesium, silicon, and iron. We note that, in the steady state, $\text{Mg/Si} = 0.70$ and $\text{Fe/Si} = 0.80$ agree with those of angrites, which are meteorites resulting from the fractional crystallisation of silicates due to impacts (see fig. 7 in Nittler et al. 2004). We also find that $\text{Cr/Fe} = 0.025$ is within Solar System (typically between 0.01–0.03; Nittler et al. 2004) and extrasolar asteroids values (e.g. Jura & Young 2014), in agreement with the hypothesis that siderophile refractory elements would condensate along with iron in rocks. The relatively low iron abundance is consistent with accretion of rocks from a thick crust and mantle of a large asteroid. Given their shorter diffusion time-scales, it may be possible that atmospheric abundances of heavier core materials (iron and nickel) were larger in the past, and these elements have now mostly diffused out of the convection zone. However, as discussed in Section 4.2 and in the following section, we argue against a long time since the end of accretion (more than a few diffusion time-scales) that would be needed to drastically change the relative abundances of metals.

In conclusion, our results suggest an intricate history for the parent body that polluted SDSS J1242, which probably underwent geological evolution, possibly caused by impacts with other asteroids. These may have caused melting and mixing of the crust, leaving a chemical signature in its composition that resemble findings for Solar System asteroids.

4.4 Oxygen excess

Since we detect all four major rock forming elements, plus minor constituents, we can assess the fraction of oxygen that was originally bound on anhydrous minerals within the parent body. We can safely exclude that the oxygen observed in the convection zone is dredged-up core-material, since all the white dwarfs that have dredged-up oxygen also show optical C I lines (see e.g. Gänsicke et al. 2010) that we do not detect. Therefore, we ignore carbon in the following discussion, but comment on its possible impact at the end of this section.

We follow Klein et al. (2010, 2011) and Farihi et al. (2011, 2013), adopting the fundamental metal-to-oxygen combinations found in rocks, i.e. Na₂O, MgO, Al₂O₃, SiO₂, CaO, TiO₂, Cr₂O₃, and FeO. Iron can also be metallic or rarely form Fe₂O₃, but we note that including only FeO in the computation is a conservative assumption, and an up-

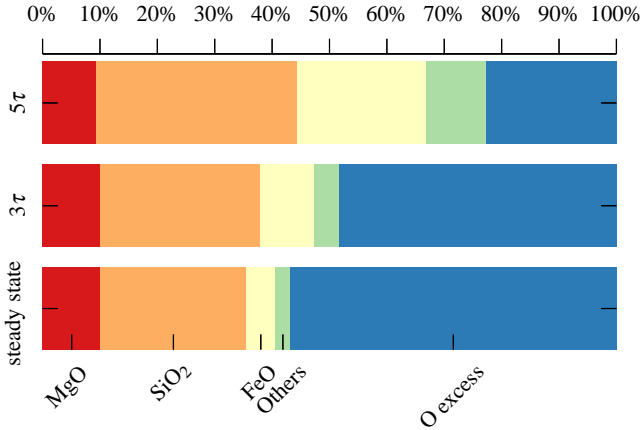


Figure 4. Oxygen balance within metal oxides at the steady state, and computed under the assumption of declining phase after 3 and 5 time-scales ($\tau \approx 1$ Myr) from the halt of the accretion. The atmospheric abundances are assumed to decrease exponentially with time. The declining phase scenario implies smaller initial oxygen excess. We now measure $M_Z = 1.2 \times 10^{24}$ g, i.e. 1.4 Ceres masses, while we would expect SDSS J1242 to have accreted at least 6×10^{24} g (7 Ceres masses), and 2×10^{25} g (1.5 Pluto masses), in the case we observe the white dwarf at 3τ and 5τ since the end of the accretion.

per limit to the number of oxygen atoms that are bound to iron. Our results are reported in Table 5. The errors are determined via a Monte Carlo method, with Gaussian probability distributions whose widths are set by the abundance uncertainties. Under the assumption of steady state, we find 57 per cent of oxygen mass to be in excess with respect to that needed to form simple anhydrous metal oxides. Because water is commonly found in asteroids, the natural explanation for this oxygen excess is that the accreted debris was rich in water ice or hydrated minerals. Taking into account the mass of metals in the convection zone of SDSS J1242, we estimate that the accreted parent body was made of 38 per cent H_2O by mass. We also note that $\text{O}/\text{Si} = 4.5$ is equivalent to the most extreme ratio measured for hydrated silicates that are found in CI and CM chondrites, which are rich in water and suspected to form in proximity of the Solar System snow line. This is a hint that the surplus oxygen may have not been carried only by rocks, but might have been bound in water ice.

If we considered instead that SDSS J1242 is observed in the decline phase, the oxygen abundance relative to other elements would change with time. Most metals that combine with oxygen diffuse faster out of the convection zone, and would have been more abundant at the end of the accretion phase. We compare in Fig. 4 the steady state oxygen balance with what could have been the parent body composition, placing the end of accretion at a few to several diffusion times in the past. We note a reduction of the oxygen excess with respect to fraction bound in metal oxides. In other words, if sufficient time has passed since the end of the accretion phase, even a dry asteroid would produce an apparent oxygen excess. However, as discussed in Section 4.2, we argue against a scenario in which SDSS J1242 is observed late in to the declining phase. Furthermore, the remarkable trace hydrogen content (Section 4.5) of this helium-dominated white

dwarf would require an additional mechanism beyond the extant pollution event.

Finally, we consider how the inclusion of solar-abundance carbon in the oxygen balance would affect our result. If carbon were found to be polluting SDSS J1242 at the upper limit, then all of the excess oxygen can be accounted for as CO_2 . However, this assumption is invalid because our optical limits are not very stringent. In the eight cases for which metal-polluted white dwarfs have been observed in the ultraviolet, their carbon abundances have been found to be at least 1000 times less abundant than the solar value (Gänsicke et al. 2012; Jura et al. 2012; Xu et al. 2014). Furthermore, only two metal-polluted white dwarf display a large abundance of carbon, the origin of which is still debated (PG 1225–079 in Xu et al. 2013, and Ton 345 in Jura et al. 2015; Wilson et al. submitted).

4.5 Hydrogen mass

Assuming that hydrogen is uniformly mixed within the convection zone of SDSS J1242, the large abundance we measure, $[\text{H}/\text{He}] = -3.68$, corresponds to $M_{\text{H}} = 2.5 \times 10^{23}$ g. Under the assumption of steady state, we have inferred that H_2O accounts for about 38 per cent of the parent-body mass, meaning that an asteroid of about 5.9×10^{24} g is needed to yield all observed M_{H} . The minimum parent body mass of 1.24×10^{24} implies that at least 5.2×10^{22} g of H was added to the envelope of SDSS J1242 in the observed accretion episode, or 20 per cent of the total M_{H} . It is possible that the entire M_{H} was accreted in this current episode, requiring steady state at the measured average rate for a few Myr. However, it cannot be excluded that multiple accretion episodes of water-rich bodies contributed to the total H-content of the envelope over the 300 Myr cooling age of the star.

We compare the M_{H} of SDSS J1242 with that of other helium-rich white dwarfs in Fig. 5, which has also been represented in different fashion and discussed in various contexts (e.g. MacDonald & Vennes 1991; Voss et al. 2007; Dufour et al. 2007; Bergeron et al. 2011). We note that SDSS J1242 holds at least one order of magnitude more hydrogen than stars with similar temperatures (i.e. cooling ages). Several hypotheses have been put forward to explain the apparent broad correlation between the hydrogen content of helium-rich white dwarfs and their effective temperature (\equiv cooling age): i) spectral type evolution, which requires the presence of small amounts of primordial hydrogen ($\lesssim 10^{-14} M_{\odot}$) that gets mixed in the helium-rich envelope once convection sets in (MacDonald & Vennes 1991; Bergeron et al. 2011); ii) accretion from the interstellar medium (ISM; Dupuis et al. 1993; Dufour et al. 2007); iii) accretion of water-rich planetary debris (Jura et al. 2009; Farihi et al. 2010a). The primordial-hydrogen hypothesis can provide the observed M_{H} of $T_{\text{eff}} \gtrsim 20\,000$ K DBA white dwarfs, but fails to explain the hydrogen content of $T_{\text{eff}} \lesssim 15\,000$ K atmospheres. The lack of hot DBA white dwarfs with large M_{H} requires an external origin for the hydrogen. Farihi et al. (2010a) strongly argued against the ISM accretion scenario, using several distinct lines of evidence, including Galactic positions and kinematics, ISM and stellar chemistry, and likely physical accretion mechanisms.

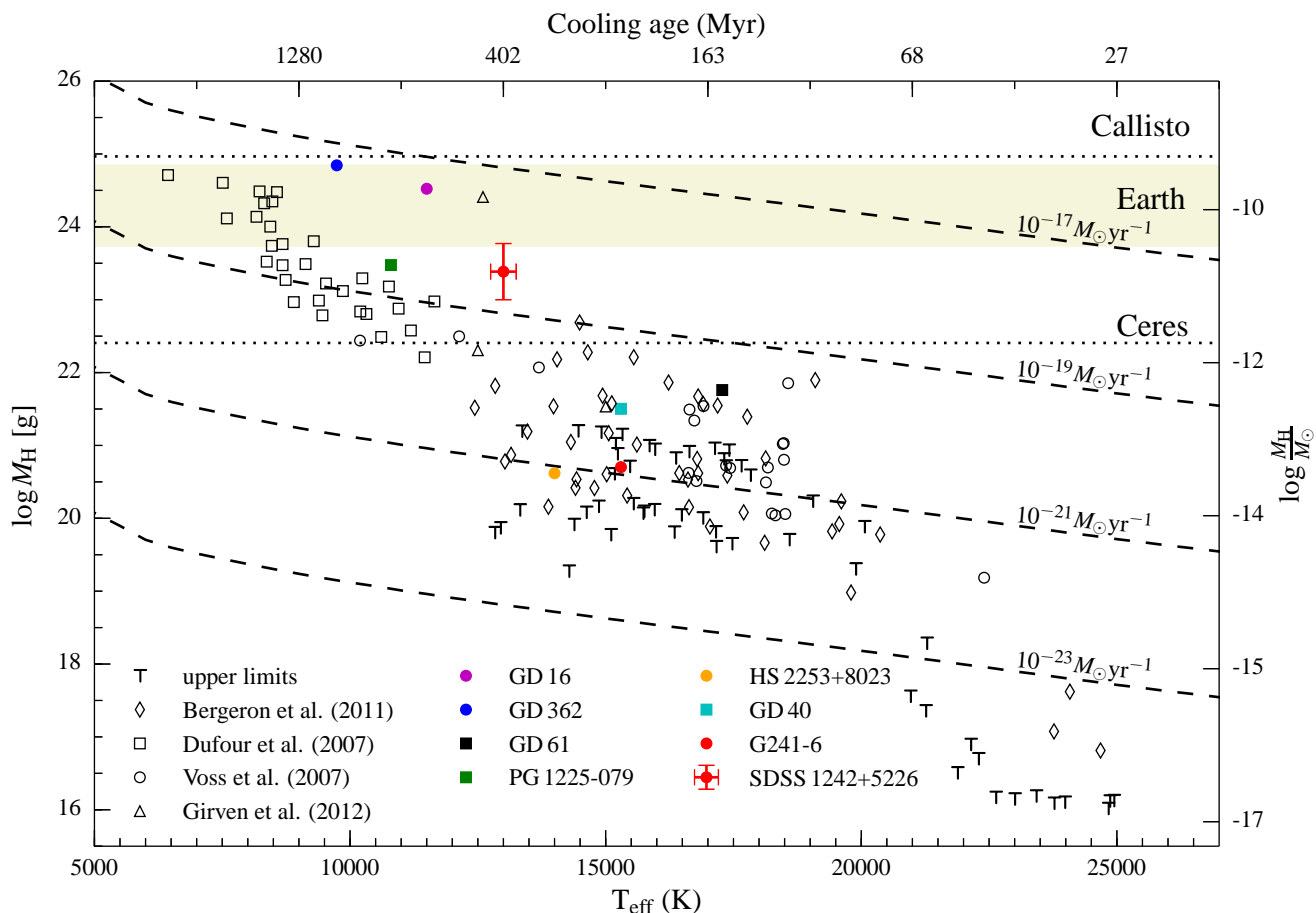


Figure 5. Total mass of hydrogen in the convection zones of helium-dominated white dwarfs as function of T_{eff} (left axis). On the right axis, the hydrogen mass is given in units of solar masses and we give the cooling age for a typical $\log g = 8$ DB white dwarf (Bergeron et al. 2011) on the top axis. Hydrogen abundances of field DBA and DZA white dwarfs (open symbols, see legend for references) were converted into hydrogen mass adopting the evolutionary models of Bergeron et al. (2011), and q_{cvz} from the updated version of Koester (2009) computations. The hydrogen abundances of metal-polluted white dwarfs are taken from Jura & Young (2014, and references therein). For GD 362 (Gianninas et al. 2004) and GD 61 (Farihi et al. 2013) we used the hydrogen mass supplied by the authors. The mass and of hydrogen in water for Ceres, Callisto (ice mass fractions are 25 and 50 per cent respectively, Michalak 2000; McCord & Sotin 2005; Canup & Ward 2002) and bulk Earth (van Thienen et al. 2007, and references therein) are plotted as dashed lines or the shaded area. The dashed curves represent the cumulative mass of hydrogen for constant accretion rates during the white dwarf cooling ages.

This also suggested that some DAZ white dwarfs are externally polluted by both metals and hydrogen.

Here we discuss additional evidence to the planetary interpretation using Fig. 5. We note that the M_{H} detected in helium-rich atmospheres spans 8–9 orders of magnitude and, if interpreted as continuous accretion from the ISM, it requires the accretion rates to be unlikely higher in old white dwarfs (dashed curves). While the observations of metal-polluted white dwarfs mainly suggests accretion of dry planetary debris (≤ 10 per cent H_2O by mass; Klein et al. 2011; Jura & Xu 2012), pollution from water-rich debris seems plausible in a handful of stars with extremely large M_{H} (GD 16, and GD 362, see Jura et al. 2009; Jura & Xu 2012), and has been confirmed in GD 61 (Farihi et al. 2013) and likely in SDSS J1242. We note that GD 16, GD 362 and SDSS J1242 are extremely metal polluted, and the first two along with GD 61 display near-infrared excess, revealing the presence of a debris disc that unambiguously con-

firms ongoing accretion. We also note that a further star possessing a large $M_{\text{H}} \approx 5 \times 10^{24}$ g is HE0446–2531 with $T_{\text{eff}} = 12600$ K. However, its spectral analysis is obtained from low-resolution spectra (Friedrich et al. 2000), and it is found not to have circumstellar disc by Girven et al. (2011). Finally, we note that about 45 per cent of the 108 helium-dominated white dwarfs analysed by Bergeron et al. (2011) show trace hydrogen, similar to the fraction of metal-polluted white dwarfs (20–30 per cent; Zuckerman et al. 2003, 2010; Koester et al. 2014). We therefore suggest that a large fraction (maybe most) of the helium-rich white dwarfs with trace hydrogen, but no signs of metal pollution, may have accreted water-rich debris in the past. The metals eventually diffuse out the convection zone once accretion ceases, while hydrogen remains in the outer, photospheric layers. Several diffusion time-scales after the end of an accretion episode, stars like GD 61, which has only a modest M_{H} in Fig. 5, will resemble a typical DBA white dwarf, while

SDSS J1242, GD 16, and GD 362 will resemble other helium-dominated white dwarfs with similar temperatures, but the larger M_{H} would be the only observable relic of their past accretion.

It is likely that extra-solar asteroids and planets, like those in our own Solar System, display a variety of compositions and water mass fractions. Water accounts for a large mass fraction of asteroids and solar-system moons (Postberg et al. 2011; Roth et al. 2014), but it is a minor constituent of inner solar-system bodies. This characteristic diversity is thought to be common place in planet formation (Bond et al. 2010) and, in the Solar System, there is evidence for an overall gradient of water content within rocky planetary bodies, increasing from the inner to the outer Solar System. The amount of water in asteroids and rocky planets is mostly determined by the initial (local) conditions constraining the snow line in the protoplanetary disc, where water condenses into ice, but it is also affected by subsequent interactions between planetary embryos (Walsh et al. 2011; Morbidelli et al. 2012). It appears that ice may survive in asteroids orbiting white dwarfs, if they are distant enough from the star to avoid engulfment during the giant branches (Mustill & Villaver 2012) and large enough to shield the internal water from the increased stellar luminosity (Jura & Xu 2010). Alternatively, water can survive in hydrated minerals that are significantly more resistant to heating. Also comets may be suggested to contribute to the fraction of M_{H} in helium-rich white dwarfs, but their delivery to the surfaces of white dwarfs should be less frequent, and have not yet been observed (Veras et al. 2014b).

4.6 Summary

The signature of water accretion on to white dwarf can exhibit as an oxygen excess (Jura & Xu 2010), and has been unambiguously confirmed in GD 61 (Farihi et al. 2013), and likely for SDSS J1242. The detailed composition analysis of SDSS J1242 has reinforced the case for water accretion in other similar white dwarfs, and possibly how that water is delivered (potentially as ice in this case). The evidence points to an asteroid once orbiting an early type main sequence star that has possibly experienced a series of impacts. We have compared its composition to that of Solar System meteorites, suggesting that the crust of the asteroid underwent geological evolution. From the magnesium and iron abundances, we suggested that melting and crystallisation of the rocks at the surface may have taken place, likely following collisions with other asteroids. Large asteroids like the one that polluted SDSS J1242, likely comparable in size or larger than Ceres, are suggested to have thick crusts made of silicates. While silicates could be important carriers of water, especially within the interior asteroids formed near or beyond the snow line, thick layers of ice are suspected to hide underneath the surface of outer main belt asteroids such as Ceres. It is therefore plausible that most of the oxygen in SDSS J1242 could have been water ice, and sufficiently deep within the parent body to prevent evaporation during the giant branches.

We stress that the discovery of stars showing oxygen excess establishes a link between the trace hydrogen observed in helium-dominated white dwarfs to the accretion of water. Studies targeting more stars with detailed abundance

analysis will be able to reveal the frequency of water-rich asteroids.

5 CONCLUSIONS

We have presented the discovery and analysis of a new, strongly metal-polluted white dwarf. We detect trace-hydrogen and eight metal species in its helium-dominated atmosphere, which we interpret as being accreted from planetary debris. The four most abundant elements are the major rock forming metals O, Mg, Si, and Fe, making up 99 per cent of the metals in the convection zone. With over 10^{24} g of metals in its outer layers and an inferred accretion rate over 10^{10} g s $^{-1}$, SDSS J1242 is one of the most polluted white dwarfs known. Its convection zone contains 2.5×10^{23} g of hydrogen, which is about an order of magnitude larger than detected in helium-dominated white dwarfs of similar temperature. From the analysis of the polluting debris, we conclude that SDSS J1242 likely accreted the remains of a water-rich planetesimal, with an H $_2$ O mass fraction of roughly 38 per cent.

With SDSS J1242, we reinforce the suggestion advanced by previous work on other strongly metal-polluted white dwarfs. These hydrogen- and oxygen-enriched stars are the metaphorical “tip of an iceberg” of water-accreting white dwarfs. A significant fraction of helium-dominated white dwarfs could accrete water-rich debris, which, accumulated over their long cooling ages, may account for the observed correlation between M_{H} and cooling age.

6 ACKNOWLEDGEMENTS

The WHT is operated on the island of La Palma by the Isaac Newton Group in the Spanish Observatorio del Roque de los Muchachos of the Instituto de Astrofísica de Canarias. The ISIS spectroscopy was obtained as part of SW2012a11 and W12AN005. LIRIS photometry was obtained as part of WHT/2011A/12. This work is based in part on observations made with the *Spitzer Space Telescope* (for program 90121), which is operated by the Jet Propulsion Laboratory, California Institute of Technology under a contract with NASA

We would like to thank Dimitri Veras for the useful discussion and for sharing the latest results of his work.

The research leading to these results has received funding from the European Research Council under the European Union’s Seventh Framework Programme (FP/2007-2013) / ERC Grant Agreement n. 320964 (WDTracer).

Funding for SDSS-III has been provided by the Alfred P. Sloan Foundation, the Participating Institutions, the National Science Foundation, and the U.S. Department of Energy Office of Science. The SDSS-III web site is <http://www.sdss3.org/>.

REFERENCES

- Abazajian K., et al., 2004, *AJ*, **128**, 502
- Abazajian K. N., et al., 2009, *ApJS*, **182**, 543
- Bergeron P., et al., 2011, *ApJ*, **737**, 28
- Bergfors C., Farihi J., Dufour P., Rocchetto M., 2014, *MNRAS*, **444**, 2147

- Bochkarev K. V., Rafikov R. R., 2011, *ApJ*, **741**, 36
- Böhm-Vitense E., 1958, *Zeitschrift für Astrophysik*, **46**, 108
- Bond J. C., O'Brien D. P., Laretta D. S., 2010, *ApJ*, **715**, 1050
- Canup R. M., Ward W. R., 2002, *AJ*, **124**, 3404
- Cardelli J. A., Clayton G. C., Mathis J. S., 1989, *ApJ*, **345**, 245
- De Sanctis M. C., et al., 2012, *Science*, **336**, 697
- Debes J. H., Sigurdsson S., 2002, *ApJ*, **572**, 556
- Dufour P., et al., 2007, *ApJ*, **663**, 1291
- Dufour P., Kilic M., Fontaine G., Bergeron P., Melis C., Bochanski J., 2012, *ApJ*, **749**, 6
- Dupuis J., Fontaine G., Pelletier C., Wesemael F., 1992, *ApJS*, **82**, 505
- Dupuis J., Fontaine G., Pelletier C., Wesemael F., 1993, *ApJS*, **84**, 73
- Eisenstein D. J., et al., 2006, *ApJS*, **167**, 40
- Falcon R. E., Winget D. E., Montgomery M. H., Williams K. A., 2012, *ApJ*, **757**, 116
- Farihi J., Jura M., Zuckerman B., 2009, *ApJ*, **694**, 805
- Farihi J., Barstow M. A., Redfield S., Dufour P., Hambly N. C., 2010a, *MNRAS*, **404**, 2123
- Farihi J., Jura M., Lee J.-E., Zuckerman B., 2010b, *ApJ*, **714**, 1386
- Farihi J., Brinkworth C. S., Gänsicke B. T., Marsh T. R., Girven J., Hoard D. W., Klein B., Koester D., 2011, *ApJ*, **728**, L8
- Farihi J., Gänsicke B. T., Steele P. R., Girven J., Burleigh M. R., Breedt E., Koester D., 2012a, *MNRAS*, **421**, 1635
- Farihi J., Gänsicke B. T., Wyatt M. C., Girven J., Pringle J. E., King A. R., 2012b, *MNRAS*, **424**, 464
- Farihi J., Gänsicke B. T., Koester D., 2013, *Science*, **342**, 218
- Fazio G. G., et al., 2004, *ApJS*, **154**, 39
- Friedrich S., Koester D., Christlieb N., Reimers D., Wisotzki L., 2000, *A&A*, **363**, 1040
- Gänsicke B. T., Marsh T. R., Southworth J., Rebassa-Mansergas A., 2006, *Science*, **314**, 1908
- Gänsicke B. T., Koester D., Marsh T. R., Rebassa-Mansergas A., Southworth J., 2008, *MNRAS*, **391**, L103
- Gänsicke B. T., Koester D., Girven J., Marsh T. R., Steeghs D., 2010, *Science*, **327**, 188
- Gänsicke B. T., Koester D., Farihi J., Girven J., Parsons S. G., Breedt E., 2012, *MNRAS*, **424**, 333
- Gianninas A., Dufour P., Bergeron P., 2004, *ApJ*, **617**, L57
- Girven J., Gänsicke B. T., Steeghs D., Koester D., 2011, *MNRAS*, **417**, 1210
- Girven J., Brinkworth C. S., Farihi J., Gänsicke B. T., Hoard D. W., Marsh T. R., Koester D., 2012, *ApJ*, **749**, 154
- Hunt L. K., Mannucci F., Testi L., Migliorini S., Stanga R. M., Baffa C., Lisi F., Vanzi L., 1998, *AJ*, **115**, 2594
- Jura M., Xu S., 2010, *AJ*, **140**, 1129
- Jura M., Xu S., 2012, *AJ*, **143**, 6
- Jura M., Young E. D., 2014, *Annual Review of Earth and Planetary Sciences*, **42**, 45
- Jura M., 2003, *ApJ*, **584**, L91
- Jura M., 2006, *ApJ*, **653**, 613
- Jura M., 2008, *AJ*, **135**, 1785
- Jura M., Farihi J., Zuckerman B., Becklin E. E., 2007, *AJ*, **133**, 1927
- Jura M., Muno M. P., Farihi J., Zuckerman B., 2009, *ApJ*, **699**, 1473
- Jura M., Xu S., Klein B., Koester D., Zuckerman B., 2012, *ApJ*, **750**, 69
- Jura M., Dufour P., Xu S., Zuckerman B., Klein B., Young E. D., Melis C., 2015, *ApJ*, **799**, 109
- Kilic M., von Hippel T., Leggett S. K., Winget D. E., 2006, *ApJ*, **646**, 474
- Klein B., Jura M., Koester D., Zuckerman B., Melis C., 2010, *ApJ*, **709**, 950
- Klein B., Jura M., Koester D., Zuckerman B., 2011, *ApJ*, **741**, 64
- Koester D., 2009, *A&A*, **498**, 517
- Koester D., 2010, *MmSAI*, **81**, 921
- Koester D., Rollenhagen K., Napiwotzki R., Voss B., Christlieb N., Homeier D., Reimers D., 2005, *A&A*, **432**, 1025
- Koester D., Gänsicke B. T., Farihi J., 2014, *A&A*, **566**, A34
- MacDonald J., Vennes S., 1991, *ApJ*, **371**, 719
- Manchado A., et al., 1998, in Fowler A. M., ed., *Society of Photo-Optical Instrumentation Engineers (SPIE) Conference Series Vol. 3354, Infrared Astronomical Instrumentation*. pp 448–455
- Marsh T. R., 1989, *PASP*, **101**, 1032
- McCord T. B., Sotin C., 2005, *Journal of Geophysical Research (Planets)*, **110**, 5009
- McDonough W. F., 2001, in *Lunar and Planetary Science Conference*. p. 2005
- Melis C., Farihi J., Dufour P., Zuckerman B., Burgasser A. J., Bergeron P., Bochanski J., Simcoe R., 2011, *ApJ*, **732**, 90
- Melis C., et al., 2012, *ApJ*, **751**, L4
- Michalak G., 2000, *A&A*, **360**, 363
- Morbidelli A., Lunine J. I., O'Brien D. P., Raymond S. N., Walsh K. J., 2012, *Annual Review of Earth and Planetary Sciences*, **40**, 251
- Morrissey P., et al., 2007, *ApJS*, **173**, 682
- Mustill A. J., Villaver E., 2012, *ApJ*, **761**, 121
- Nittler L. R., McCoy T. J., Clark P. E., Murphy M. E., Trombka J. I., Jarosewich E., 2004, *Antarctic Meteorite Research*, **17**, 231
- Postberg F., Schmidt J., Hillier J., Kempf S., Srama R., 2011, *Nature*, **474**, 620
- Reach W. T., Kuchner M. J., von Hippel T., Burrows A., Mullally F., Kilic M., Winget D. E., 2005, *ApJ*, **635**, L161
- Rocchetto M., Farihi J., Gänsicke B. T., Bergfors C., 2014, *ArXiv e-prints*,
- Roth L., Saur J., Retherford K. D., Strobel D. F., Feldman P. D., McGrath M. A., Nimmo F., 2014, *Science*, **343**, 171
- Schatzman E., 1945, *Annales d'Astrophysique*, **8**, 143
- Schatzman E., 1947, *Annales d'Astrophysique*, **10**, 19
- Schlegel D. J., Finkbeiner D. P., Davis M., 1998, *ApJ*, **500**, 525
- Sion E. M., Greenstein J. L., Landstreet J. D., Liebert J., Shipman H. L., Wegner G. A., 1983, *ApJ*, **269**, 253
- Tremblay P.-E., Ludwig H.-G., Steffen M., Freytag B., 2013, *A&A*, **559**, A104
- Vennes S., Kawka A., Németh P., 2010, *MNRAS*, **404**, L40
- Veras D., Mustill A. J., Bonsor A., Wyatt M. C., 2013, *MNRAS*, **431**, 1686
- Veras D., Leinhardt Z. M., Bonsor A., Gänsicke B. T., 2014a, *MNRAS*, **445**, 2244

- Veras D., Shannon A., Gänsicke B. T., 2014b, *MNRAS*, **445**, 4175
- Voss B., Koester D., Napiwotzki R., Christlieb N., Reimers D., 2007, *A&A*, **470**, 1079
- Walsh K. J., Morbidelli A., Raymond S. N., O'Brien D. P., Mandell A. M., 2011, *Nature*, **475**, 206
- Werner M. W., et al., 2004, *ApJS*, **154**, 1
- Wilson D. J., Gänsicke B. T., Koester D., Raddi R., Breedt E., Southworth J., Parsons S. G., 2014, *MNRAS*, **445**, 1878
- Xu S., Jura M., Klein B., Koester D., Zuckerman B., 2013, *ApJ*, **766**, 132
- Xu S., Jura M., Koester D., Klein B., Zuckerman B., 2014, *ApJ*, **783**, 79
- York D. G., et al., 2000, *AJ*, **120**, 1579
- Zuckerman B., Koester D., Reid I. N., Hüensch M., 2003, *ApJ*, **596**, 477
- Zuckerman B., Koester D., Melis C., Hansen B. M., Jura M., 2007, *ApJ*, **671**, 872
- Zuckerman B., Melis C., Klein B., Koester D., Jura M., 2010, *ApJ*, **722**, 725
- van Thienen P., Benzerara K., Breuer D., Gillmann C., Labrosse S., Lognonné P., Spohn T., 2007, *SSRv*, **129**, 167